LA-UR-15-21827
Approved for public release; distribution is unlimited.

Title: Anisotropy in the Ratchet Growth of PBX 9502

Author(s): Schwarz, Ricardo Blum
Liu, Cheng
Thompson, Darla Graff

Intended for: Report

Issued: 2015-03-12

Anisotropy in the Ratchet Growth of PBX 9502

R.B. Schwarz (1), Cheng Liu (1), and Darla G. Thompson (2)

(1) MST Division, Group MST-8
(2) WX Division, Group WX-7
Los Alamos National Laboratory
Los Alamos, NM 87504.

3/9/2015

ABSTRACT

TATB-based compactions and composites are known to undergo “ratchet growth”, an irreversible volume increase that occurs upon heating or cooling of a specimen. Ratchet growth likely arises because the coefficient of thermal expansion of the TATB crystals is strongly anisotropic, but the exact mechanism is not well-understood. TATB crystals in solid, plastic-bonded, explosive PBX 9502 parts can have a preferred crystallographic orientation (texture) caused by the compaction process. As a result, the irreversible strain associated with PBX 9502 ratchet growth is anisotropic. The present paper relates the magnitude of ratchet growth to the crystalline anisotropy of the TATB crystals. The crystalline anisotropy is measured by x-ray diffraction and the ratchet growth is measured by a digital image-correlation technique.

1. INTRODUCTION

The present study was done on PBX 9502, a modern insensitive explosive. PBX 9502 is a composite of 95 wt. % TATB crystals and 5 wt.% KelF-800. The Kel-F polymer is amorphous, and is added as a bonding agent. The polymer has a glass-transition temperature of 302 K.[1] Like many PBX composites, PBX 9502 is first produced as a molding powder, then heated and compressed (either isostatically or in dies) to produce solid parts that can be machined.

TATB crystals, 1, 3, 5-triamino-2, 4, 6,-trinitrobenzene [2], have triclinic structure (space group *P*-1), with lattice parameters $a_o = b_o = 0.903$ nm, $c_o = 0.681$ nm, $\alpha = 108.6^o$, $\beta = 91.8^o$, and $\gamma = 120.0^o$ [3]. Figure 1 is an SEM picture of a mechanically induced fracture surface of a TATB aggregate. Each TATB crystal is composed of many parallel lamellae, each approximately 0.4 μm thick. The plane of each lamellae is parallel to the (002) crystallographic (basal) plane of the triclinic structure. Because $\alpha \neq \beta$, there are three lattice variants in the crystal, each lamella having a slightly different c-axis, which revolves about the normal to the basal plane.[3]

It has long been known that, similarly to pure TATB, when a pressed PBX 9502 parts is heated, its volume grows *irreversibly*. Experience has shown that the phenomenon is augmented and accelerated if the heating is done in cyclic fashion, interlaced with cooling cycles.[4] The

irreversible growth developed in this manner had been denoted as *Ratchet Growth* and, after a dozen or so cycles between -50 and 100^{o}C, it can amount to a permanent decrease in density of several percent. Ratchet Growth is asymptotic in nature, with most of the growth occurring in the first few cycles, tapering off significantly after 25-30 cycles. It has also been observed that the extent of Ratchet Growth in polycrystalline TATB materials is affected by crystallographic texture in the part.[5]

Crystals with less-than-cubic symmetry generally have different linear thermal expansion coefficients along the three axes that characterize the crystal unit cell. Furthermore, in monoclinic and triclinic crystals, the angles between these axes may also change with changing temperature. Kolb and Rizzo [6] used x-ray diffraction to measure the coefficients of thermal expansion (CTE) of TATB between -59 and 104^{o}C. They found it to be highly anisotropic: 8.3 x 10^{-6} K^{-1}, 20. 9 x 10^{-6} K^{-1}, and 248 x 10^{-6} K^{-1} along the *a, b,* and *c* unit-cell axes, respectively. This large anisotropy in CTE was attributed to its atomic structure. As first reported by Cady and Larson [7], the TATB molecules are based on benzene rings, which are oriented parallel to the (002) basal planes. These rings are terminated with nitro and amine groups. Relatively strong hydrogen bond tie the benzene rings within the basal (002) planes, whereas weak van der Waals bonds tie the benzene rings normal to the basal planes, along the crystallographic z-axis.

The different type of atomic bonding present along and normal to the basal planes of a TATB crystal suggests that its elastic and plastic properties are anisotropic. But, because defect-free, mm-size, TATB crystals have been found quite difficult to grow, these properties have not yet been measured. The elastic properties of TATB have been calculated using molecular dynamics [8] and density functional theory [9] and these results do predict a large anisotropy in the elastic properties. There are no reports on the plastic properties of a TATB crystal. However, the large difference between the atomic bond strength along and normal to the basal plane suggests that the TATB crystals deform primarily by shear along the (002) basal planes. Additional deformation by twinning has also been observed [10].

Although the CTE of a TATB *single crystal* is strongly anisotropic,[6] after a TATB crystal has been thermally cycled, it returns to its original shape, retaining no internal stresses. The situation is quite different for a pressed compact of polycrystalline TATB. When this solid

is heated or cooled, each crystal in the aggregate wants to expand preferentially along its own [002] lattice direction. The failure of neighboring grains to fit together properly develops internal stresses, which change in magnitude and direction from grain to grain. These stresses are called "tessellated stresses" [11] to distinguish them from the "body stresses" that are generated by external forces, or due to self-strain, and which spread uniformly over regions containing many grains.

Tessellated stresses are a rather common phenomenon. They also develop, for example, in polycrystalline aggregates made of grains having cubic symmetry (e.g. iron) when such an aggregate is loaded within the elastic limit. Here, the thermal expansion in each grain is isotropic but its elastic properties are not. Then, upon applying an external load, tessellated stresses develop because the Young's modulus of a given grain does not necessarily match those of its adjacent grains. Therefore, most solids prepared by the compaction of powder retain some degree of tessellated stresses, which may be partially reduced by a slow thermal anneal. (An exception may be compacted polycrystalline tungsten, since its grains are almost elastically isotropic). Whatever its origin, if on reducing the compacting pressure the tessellated stresses exceed the interparticle strength, the aggregate will develop cracks and/or voids whose dimensions will mimic those of the grains.

There is yet no clear model to explain ratchet growth in TATB aggregates. We thus hypothesize the following.[12] Because the elastic properties of each TATB crystal are highly anisotropic, on reducing the applied compaction pressure, the TATB solid will develop strong tessellated stresses, leading to the creation of cracks and voids. Thus, the production of a crack-free, fully dense, TATB compact is highly unlikely. If the temperature of the compact is now changed, either by heating or cooling from the value at which it was pressed, the distribution of tessellated stresses will change. Both compressive and tensile stresses will be generated, which average zero. At some locations, the local tensile stresses will exceed the interparticle strength, leading to the creation of additional voids. Because the locations where the tessellated stresses exceed the interparticle strength on heating are not necessarily the same locations where it exceeds it on cooling, a different set of voids will be created on heating than on cooling. Both heating and cooling with produce voids, and thus both should lead to a cumulative decrease in the density of the pressed polycrystalline TATB part.

Subsequent heating and cooling cycles may reshuffle the distribution of tessellated stresses and lead to additional volume increases of ever decreasing amplitude.

When the heating/cooling sequence is applied in cyclic fashion, the resulting volume increase is called ratchet growth. Ratchet growth has been observed in both die-pressed and isostatically pressed TATB parts, and extensive work has been done to quantify it and to develop a better theoretical understanding.[13,14] Pressed graphite composites have been observed to display similar cyclic growth behavior.[15]

In PBX 9502 parts fabricated by pressing powder, the TATB crystals usually have preferential orientations (texture), which vary from point to point in the part. The texture introduces noticeable anisotropy in both the CTE of the part and in the amplitude of its ratchet growth. The presence of anisotropy in the CTE of PBX 9502 parts was first reported in [16,17]. Recently, Schwarz et al. related the anisotropy in the CTE to the crystallographic texture in the part.[12] The present work relates the anisotropy in the ratchet growth of PBX 9502 to its crystallographic texture.

Crystallographic texture at any given location in the specimen is usually represented by an Orientation Distribution Function, *ODF*. This function defines the volume fraction of grains with a certain orientation $\boldsymbol{g}$.

$$ODF(g)=\frac{1}{V}\frac{dV(g)}{dg} \tag{1}$$

The orientation $\boldsymbol{g}$ is normally identified using three Euler angles, which describe the transition from the sample's reference frame to the crystallographic reference frame of each individual grain in the polycrystal.

Traditionally, both X-ray diffraction and electron back-scattering diffraction methods have been used to collect descriptions of the texture, which are first represented in "pole figures". Different methodologies exist to obtain the ODF from a combination of pole figures, each giving us a complimentary, partial-view, of the general texture.[18]

For the present case of PBX 9502, however, the situation is much simpler. Because the TATB crystals in PBX 9502 are graphitic in nature (with effectively only one slip mode parallel to the TATB basal planes), the main texture we expect in this material is a preferential reorientation of the (002) basal planes of TATB. We will assume this to be true, and this assumption will be corroborated by the present results. This means that a rather complete description of the texture state of the PBX 9502 material can be obtained from a *single* pole figure for the (002) Bragg reflection of TATB.

2. EXPERIMENTAL

The present study was done on a disk-shaped specimen of PBX 9502, 12.5 mm diameter and 1.42 mm thick. The *as-pressed* disk had a density of 1.902 g cm^{-3}, approximately 98% of the theoretical maximum density of TATB, 1.942 g cm^{-3} [19]. The density of the KelF-800 polymeric binder is approximately 2.02 g cm^{-3}[1], quite similar to that of TATB. Thus, the as-fabricated specimen (before Ratchet Growth) had approximately 2% porosity. The disk was cut from a larger semi-spherical piece that was fabricated by pressing molding powder (each particle being a fine mixture of TATB crystals and the KelF-800 binder) against a spherical mandrel. The pressing was done at approximately 50^{o}C. During consolidation, the pressed part develops crystallographic texture because the TATB crystallites rotate by various amounts in response to the applied compacting pressure, the presence of the solid mandrel, and the fact that each TATB crystal deforms effectively by shear parallel to its basal plane.

A right-handed x-y-z reference coordinate system is attached to the disk-shaped specimen, as shown in Fig. 2. It is defined with the z-axis normal to the disk surface. The origin of the triad is at the disk center. The x-axis is contained in the plane of the disk, passing through a reference point painted on its cylindrical surface. This point defines the $\delta = 0$ value. In Fig. 3, the condition $\delta = 0$ corresponds to the *x*-axis is pointing up.

In this paper we used three experimental techniques: (1) transmission x-ray diffraction to collect texture data, which we represent in a (002) pole figure; (2) thermal analysis, which we use to measure the thermal expansion of the specimen as a function of orientation; and (3) digital image correlation analysis, which we used to measure the Ratchet Growth as a function of

orientation. These three techniques were applied to the same specimen. The techniques are described next.

Figure 3 is a schematic describing the collection of x-ray diffraction data in PBX 9502. Because this material has a relatively low absorption coefficient for x-rays, the diffraction data cannot be collected in a reflection mode, which is the traditional method used to obtain texture data for metals and alloys. Instead, we used the transmission method of Decker, Asp and Harker [20], where x-ray diffraction data at a constant diffracting angle 2θ is collected on a specimen of uniform thickness. As shown schematically in Fig. 3, the disk-shaped sample is rotated continuously by an angle δ about the *Z*-axis, normal to the sample surface. Simultaneously, the "generator" angle, Ω, and the "detector" angle, ϕ, are both incremented, while keeping the difference $\Omega - \phi = 2\theta$ = constant. The result is a set of values for the diffracted intensity as a function of the angles δ and α, where $\alpha = \Omega - \theta$ (the dash-dot line bisects the angle 2θ). This data is then used to construct a "pole figure" for the particular diffracting angle, 2θ. In our tests, the disk-shaped specimens were rotated at the speed $d\delta/dt$ = 1 deg/sec. At the same time, the angle α was incremented at the speed $d\alpha/dt$ = 0.01 deg/sec. The diffracting angle was fixed at $2\theta = 28.41^{o}$, corresponding to the (002) Bragg reflection of TATB. The inset to Fig. 2 shows how a single datum, obtained at a particular value of δ and α, is located on a polar plot to construct the "pole figure". Because $d\alpha/dt << d\delta/dt$, the pole figure is constructed via the accumulation of data along a spiral of continually decreasing radius (continuously increasing α).

Geometrical constraints inherent to the transmission method (above a critical value of the angle α, the x-ray beam collides with parts of the goniometer holding the specimen) limited our data collection to the range $0 < \alpha < 38.2^{o}$. Thus, the transmission method (based on a single specimen), does not enable us to fill the center region of the pole figure. To determine the complete pole figure would require we convolute transmission diffraction data collected from various thin specimens cut at different angles from the same region of the solid. This α-range limitation, however, has no consequence in the present analysis since, as we shall see, the missing data (that for the range $38.2^{o} < \alpha < 90^{o}$) has no intensity maxima. Furthermore, the missing data can be inferred from an extrapolation of the available data, for $0 < \alpha < 38.2^{o}$.

The coefficient of thermal expansion (CTE) of the PBX 9502 specimen was measured using a TA Instruments Thermal Mechanical Analyzer, Model Q400 (New Castle, DE, USA). The CTE was measured across many sample diameters (by varying stepwise the angle δ defined in Fig. 2). The CTE was also measured across the sample thickness.

The (irreversible) strain caused by ratchet growth was determined using a digital-image-correlation (DIC) technique. These measurements consisted of the following steps: (1) Spray-paint a fine speckle pattern on the flat surface of the PBX 9502 disk; (2) At 25^{o}C, take an initial digital picture of the speckle pattern; (3) Subject the disk to eight thermal cycles between -55^{o}C and 75^{o}C, heating and cooling at 1 K min^{-1} , and holding at the extreme temperatures for 15 minutes; (4) Upon returning to 25^{o}C, take a second digital picture of the speckle pattern; (5) process the two digital patterns to obtain the deformation field; and (6) deduce the six components of the (irreversible) strain generated by the cyclic heating-cooling.

2. RESULTS

Figure 4 is a polar projection of the (002) Bragg intensity in our disk-shaped specimen of PBX 9502. This pole figure has two pronounced maxima at ($\alpha = 0$, $\delta = 30^{o}$) and ($\alpha = 0$, $\delta = 210^{o}$). Figures 2 and 3 help us understand the pole figure.

With respect to Fig. 3, the dash-dot line that bisects the angle 2θ gives the orientation of the (0,0,2) crystallographic planes that are currently contributing to the x-ray diffracted intensity being collected by the detector. Therefore, points on the outer ring of the pole figure, for $\alpha = 0$, denote the relative density of TATB crystals in the disk-shaped specimen that have (002) planes oriented *normal* to the surface of the disk. Similarly, the single datum at the center of the pole figure, for $\alpha = 90$ deg., measures the relative density of (002) planes oriented *parallel* to the disk surface. As stated before, geometrical constraints, inherent to the present transmission method, limit our data collection to the range $0 < \alpha < 38.2$ degree.

The three parallel traces in Fig. 2 indicate the preferred orientation of the (002) planes of TATB in the specimen. These surfaces are normal to the geometric *X*-*Y* surface (they contain the *Z* direction). As the angle delta increases, the diffracted intensity has a maximum every time the preferred (002) planes of TATB are parallel to the geometric plane *Y*-*Z*.

Figure 5 is a polar plot of the CTE of PBX 9502 disk, measured across the disk diameter. The CTE on the plane of the disk is clearly anisotropic, ranging from approximately 50 x 10^{-6} to 81 x 10^{-6}. It has a two-fold symmetry consistent with the TATB texture in the PBX 9502 disk: the CTE value is largest when measured normal to the preferential orientation of the (002) planes, and smallest when measured along the (002) planes. The CTE measured normal to the plane of the disk was approximately 45 x 10^{-6}. Therefore, the CTE for this PBX 9502 specimen sample can be represented by an ellipsoid with major axes of approximately 50, 50, and 80 x 10^{-6}.[5]

Figure 6 shows speckle patterns recorded on the flat surface of the specimen before and after the thermal cycling, respectively. These digital images have a spatial resolution of 8 μm/pixel. To correlate the two images, the DIC analysis starts by identifying corresponding sub-cells, each approximately 45 pixels in diameter, which corresponds to circular regions of approximately 0.35 mm diameter. This process generates a pair of corresponding points in the two images. The process is repeated at adjacent regions of the images. The DIC analysis generated approximately 61,000 pairs of corresponding data points between the two images in Fig. 6. We developed a least squares code to determine accurately the rigid translation and rotations between these two images. Removing these displacements, we are left with the displacement field induced by the ratchet growth onto the surface of the specimen. Ratchet growth also affects the thickness of the specimen. For the present texture, shown in Figs. 4, we expect the thickness increase to be uniform across the surface.

3. DISCUSSION.

3.1. Displacement fields

Figure 7 is a polar plot of the measured radial component of the deformation field, u_r , at the surface of the disk. We determined that this pattern is independent of the choice of origin on the disk. Notice that the *gradient* in u_r is largest in the angular direction of approximately $\delta \approx 35^o$, in agreement with the direction for which the CTE in Fig. 3 in maximum. Figure 8 is a linear plot of the ratio u_r/r , for all points on the disk surface. Because this ratio is a function of θ only, it implies that $u_r/r = \partial u_r/\partial r = \varepsilon_{rr}$. We least-squares fitted to these data the function

$\varepsilon_{rr} = \varepsilon_o + \varepsilon_1 \cos(2\theta - \theta_r)$, shown in Fig. 8 as a solid curve. The fitting parameters are given in Table 1.

Figure 9 is a polar plot of the measured angular displacement, $\Delta\theta$, at the surface of the disk. Clearly, the angular displacements are a function of the angle θ only. This is confirmed in Fig. 10, which is a linear plot of the angular displacement, $\Delta\theta$ (in degree) as a function of the angle θ. The plot includes all pixel data for the disk surface. Notice that $\Delta\theta$ assumes positive and negative values. We fitted to these data the equation $\Delta\theta = \Delta_o + \Delta_1 \sin(2\theta - \theta_\theta)$, shown as a solid curve. The fitting parameters are also given in Table 1.

3.2. Strain components describing ratchet growth

The six components of the strain tensor that describe the ratchet growth can be derived from the displacement fields. In cylindrical coordinates,

$$\epsilon_{rr} = \frac{\partial u_r}{\partial r} \tag{2}$$

$$\epsilon_{\theta\theta} = \frac{1}{r}\left(\frac{\partial u_\theta}{\partial \theta} + u_r\right) \tag{3}$$

$$\epsilon_{zz} = \frac{\partial u_z}{\partial z} \tag{4}$$

$$\epsilon_{r\theta} = \frac{1}{2}\left(\frac{1}{r}\frac{\partial u_r}{\partial \theta} + \frac{\partial u_\theta}{\partial r} - \frac{u_\theta}{r}\right) \tag{5}$$

$$\epsilon_{\theta z} = \frac{1}{2}\left(\frac{\partial u_\theta}{\partial r} + \frac{1}{r}\frac{\partial u_z}{\partial \theta}\right) \tag{6}$$

$$\epsilon_{zr} = \frac{1}{2}\left(\frac{\partial u_r}{\partial z} + \frac{\partial u_z}{\partial r}\right) \tag{7}$$

where $u_\theta = r\,\Delta\theta$, with $\Delta\theta$ in radians . Using the analytical functions we previously fitted to the u_r/r and $\Delta\theta$ data, we used the definitions above to derive:

$$\varepsilon_{rr} = 0.0064 + 0.0029 \cos(2\theta - 70.4^o) \tag{8}$$

$$\varepsilon_{\theta\theta} = -0.0059 \cos(2\theta - 69.99^o) + 0.0064 + 0.0029 \cos(2\theta - 70.3^o) \tag{9}$$

$$\varepsilon_{r\theta} = -0.0064 \sin(2\theta - 70.3^o) \tag{10}$$

Figure 11 shows a polar plot of the radial strain due to the Ratchet Growth. In comparing this figure with the plot for the thermal expansion in Fig. 5, we notice that whereas the CTE is well represented by an ellipse (ellipsoid in three dimensions), the radial strain is represented by a double cardioid.

Figure 12 shows linear plots of the three components of strain, $\varepsilon_{rr}(\theta)$, $\varepsilon_{\theta\theta}(\theta)$,and $\varepsilon_{r\theta}(\theta)$, as calculated in Eqs.(8), (9), and (10). The four vertical, dotted, lines denote the angle values at which the *shear* strain component, $\varepsilon_{r\theta}(\theta)$, is zero. These angles define the principal directions at which the strain components $\varepsilon_{rr}(\theta)$ and $\varepsilon_{\theta\theta}(\theta)$ assume extreme values. These are $\theta = 35.15^{o}$ and $\theta = 125.15^{o}$.

The dilation of the disk on its flat surface is given by the surface strain, $\Delta A/A = \varepsilon_{rr} + \varepsilon_{\theta\theta}$. $\Delta A/A$ is approximately constant and equal to 0.0128.

With the present DIC technique, we only measured the displacement fields in the surface of the disk, both on the r and θ directions. We did not measure the displacement field in the z direction, normal to the disk. This would have required spray painting the lateral (cylindrical) surface of the disk, and the more complicated acquisition of digital images on a curved surface. Lacking this information, we cannot use equations (4), (5), and (6), to determine the ε_{zz}, $\varepsilon_{\theta z}$, and ε_{zr} components of strain due to ratchet growth. However, the fact that our sample had a simple crystallographic texture, as illustrated in Fig. 4, allowed us to deduce these components in an indirect manner. The key to this was to visualize the displacement field $u_z(r,\theta,z)$. Microscopy studies [21] of the PBX 9502 starting powder material reveals that each powder particle contains a seemingly random distribution of plate-like TATB crystals. The lateral dimensions of these plates are 60 – 100 μm, whereas their thickness is much smaller, 1 - 20 μm. The texture we measure in pressed parts of PBX 9502 is the result of reorientations of the plate-like crystallites during powder consolidation. Our texture and CTE data suggest that the crystallographic texture in the present PBX 9502 specimen is rather simple, and can be described by a *single* (002) crystallographic pole. In the (X, Y, Z) Cartesian coordinate system of Fig. 2, this (002) pole is parallel to the (X,Y) plane, making an angle of approximately 35 degree with the X-axis. (Note that in this figure, the (002) texture *pole* is normal to the planes defined by the three thin traces added to the disk).

We then conclude that the strain caused by ratchet growth along a plane *normal* to the (002) texture pole is independent of the direction on that plane. In other words, if we look at surfaces defined by the thin lines in Fig.2 (which contain the direction *Z*), and ask what is the radial strain along any direction contained on those planes, the answer is the same.

From symmetry, it then follows that for $\theta = 35.1 + 90 = 125.1^{o}$, ε_{zz} equals ε_{rr}. Therefore, $\varepsilon_{zz} = 0.0035$. The displacement field, $u_{zz} = 0.0035\, z$. It follows from Eqs. (5) and (6) that the shear components $\varepsilon_{\theta z}$ and ε_{zr} are both equal to zero.

The volumetric strain is:

$$\frac{\Delta V}{V} = \epsilon_{rr} + \epsilon_{\theta\theta} + \epsilon_{zz} = 0.0128 + 0.0035 = 0.0163 \qquad (10)$$

Figure 13 illustrates the anisotropy in the volume change of a disk, initially perfectly cylindrical, as the result of ratchet growth.

4. CONCLUSIONS

We have used the DIC method to derive all six components of strain due to ratchet growth in PBX 9502 caused by repeated heating and cooling (8 cycles between -55 and 75^{o}C). A careful choice of the sample orientation was essential in these studies because it simplified the analysis significantly. We chose a disk-shaped specimen having the (002) pole contained on the plane of the disk. This particular texture orientation simplified the analytical expressions for the strain components and enabled us to deduce the ε_{zz} strain component (normal to the disk surface) from the measured ε_{rr} strain component along a particular direction on the surface of the disk. o ensure that the sample has this particular orientation, texture measurements should be performed concurrently with the measurements of strain via the DIC technique, as we have done here.

The present thermal cycling (8 cycles between -55 and 75^{o}C) caused the density of the PBX 9502 disk to decreases uniformly by 1.63%. Although the decrease in density is isotropic (it is approximately the same at each point in the specimen), the strain due to ratchet growth is anisotropic. Thus, in the presence of texture, thermal cycling causes the PBX 9502 disk not only to increase in volume, but also to change shape, as shown in Fig. 13. The shape change is a direct consequence of the texture.

There is a clear similarity between the angular dependence of the CTE (shown in Fig. 5), which represents a *reversible* deformation, and the angular dependence of the ratchet growth (shown in Fig. 13), which is an *irreversible* shape change. Both effects are due to the anisotropy in the coefficient of thermal expansion of the TATB crystal and the fact that these crystals have a preferred orientation (texture) in PBX 9502.

The present study was facilitated by the simplicity of the TATB texture in PBX 9502, enabling us to characterize it by a single (002) pole, an assumption we made at the onset of this study. There is no reason to assume that PBX 9502 has this type of texture, except the fact that the TATB crystals have a graphitic-like structure. The results to date (anisotropy of the CTE and ratchet growth strain) support this assumption. In general, this simple assumption cannot be made. The texture that develops in deformed polycrystalline aluminum, for example, is quite complicated and depends on the deformation path. In these cases, an analysis of the texture, and its effects, requires the measurement of a number of pole figures for various diffracting angles.

The solid lines in figures 8, 10 and 11 are analytical curves that were least-squares fitted to all the DIC data collected on the surface of the disk-shaped specimen. Although these curves give a rather good representation of the data, clearly there are small systematic deviations. Various factors could be contributing to these deviations: (a) the data cannot be fitted by simple sinusoidal functions, as we have done here. For example, the dependence of the texture intensity on angle θ may be better represented by a Gaussian function in θ, rather than by a simple sine function; (b) the texture is not the same at all points in the cylindrical specimen. This specimen was cut from a larger part, which had been fabricated by isostatic compaction. Most likely, the density and texture in the as-fabricated part are slightly inhomogeneous; and (c) the (002) pole characterizing the texture is not perfectly normal to the z-axis (see Fig. 2.). The texture data in Fig. 4 does not allow us to detect an angular deviation of a few degrees. In hindsight, the normality between the (002) pole axis and the z-axis (normal to the specimen's face) could be better established if the texture measurements in Fig. 4 were to include data for negative values of α. Future texture measurements will include these data.

Acknowledgement:
This work was supported by the Enhanced Surveillance Program at LANL, led by Thomas Zocco. LANL is operated by LANS, LLC, under DOE/NNSA contract DE-AC52-06NA25396.

REFERENCES

1. B. M. Dobratz, "LLNL Explosives Handbook", Lawrence Livermore National Laboratory, publication UCRL-52997, March 1981.
2. T. M. Benziger and R. K. Rohwer, "*Pilot Plant Production of Triaminonitrobenzene (TATB)*", Los Alamos Scientific Laboratory Report, LA-3632, 1967.
3. Howard H. Cady, "Crystallographic Data", The Microscope & Crystal Front 14 (1963) 57.
4. H. H. Cady, "Ratchet Growth in PBX 9502", 30th Meeting of JOWOG-9, October 9-13, 1989
5. R. B. Schwarz, G. W. Brown, D. G. Thompson, B. W. Olinger, J. Furmanski, and H. H. Cady "The Effect of Shear Strain on Texture in Pressed Plastic Bonded Explosives", Propellants Explos. Pyrothech., 38 (2013) 685-694.
6. John R. Kolb and H. F. Rizzo, "Growth of 1, 3, 5-triamino-2, 4, 6,-trinitrobenzene (TATB) I. Anisotropic Thermal Expansion", Propellants and Explosives 4, (1979) 10-16.
7. H. H. Cady and A. C. Larson, Acta Crystallogr. Part 3, 18, 485 (1965).
8. D. Bedrov, O. Borodin, G. D. Smith, T. D. Sewell, D. M. Dattelbaum, and L. L. Stevens, "*A molecular dynamics simulation study of crystalline 1,2,5-triamino2-,4,6-trinitrobenzene as a function of pressure and temperature*", J. Chem. Phys. 131, 224703(2009).
9. L. Valenzano, W. J. Slough, and W. F. Perger, "Accurate Prediction of second order elastic constants from first principles: PETN and TATB", Shock Compress. Condens. Matter, Amer. Phys. Soc. 1426 (2011) 1191-1194.
10. C. B. Skidmore, D. S. Phillips, and N. B. Crane, "*Microscopical Examination of plastic-bonded explosives*", Microscope 45 (1997) 127-136.
11. F. László, *J. Iron Steel Ins.* 147 (1943) 173; 148 (1943) 137; 150 (1944) 183; 152 (1945) 207.
12. R. B. Schwarz, unpublished results, Los Alamos National Laboratory, 2015.
13. D. G. Thompson, G. W. Brown, B. Olinger, J. T. Mang, B. Patterson, R. DeLuca, and S. Hagelberg, "The Effects of TATB Ratchet Growth on PBX 9502, Propellants, Explos. Pyrotech. 2010, 35, 507-513.

14. D. G. Thompson, R. B. Schwarz, G. W. Brown, R. DeLuca, “Time-Evolution of TATB-Based Irreversible Thermal Expansion (Ratchet Growth), Propellants Explos. Pyrotech., accepted for publication, November 2014.
15. R. G. Naum and C. K. Jun, “Thermal expansion of polycrystalline graphite”, J. Appl;. Phys. 4 (1970) 10.
16. Jon L. Maienschein and F. Garcia, “Thermal Expansion of TATB-based Explosives from 300 to 566 K”, Thermochimica Acta 384 (2002) 71-83.
17. Cary B. Skidmore, Thomas A. Butler, Cynthia W. Sandoval, “The elusive Coefficient of Thermal Expansion of PBX 9502”, Los Alamos National Laboratory Report LA-14003, National Technical Information Service, U.S. Department of Commerce, 5285 Port Royal Rd., Springfield, VA 22616.
18. U. F. Kocks, C.N. Tome, and H.-R. Wenk, “Texture and Anisotropy”, (Cambridge University Press, 1998).
19. B. Olinger, “Compacting Plastic-Bonded Explosive Molding Powders to Dense Solids”, Los Alamos National Laboratory Report LA-14173, August 2005.
20. B. F. Decker, E. T. Asp, and D. Harker, “Preferred Orientation Determination Using a Geiger Counter X-Ray Diffraction Goniometer”, J. Appl. Phys. 19 (1948) 388.
21. C. B. Skidmore, D. S. Phillips, and N. B. Crane, “Microscopical Examination of Plastic-Bonded Explosives”, Microscope, 45 (1997) 127-136.

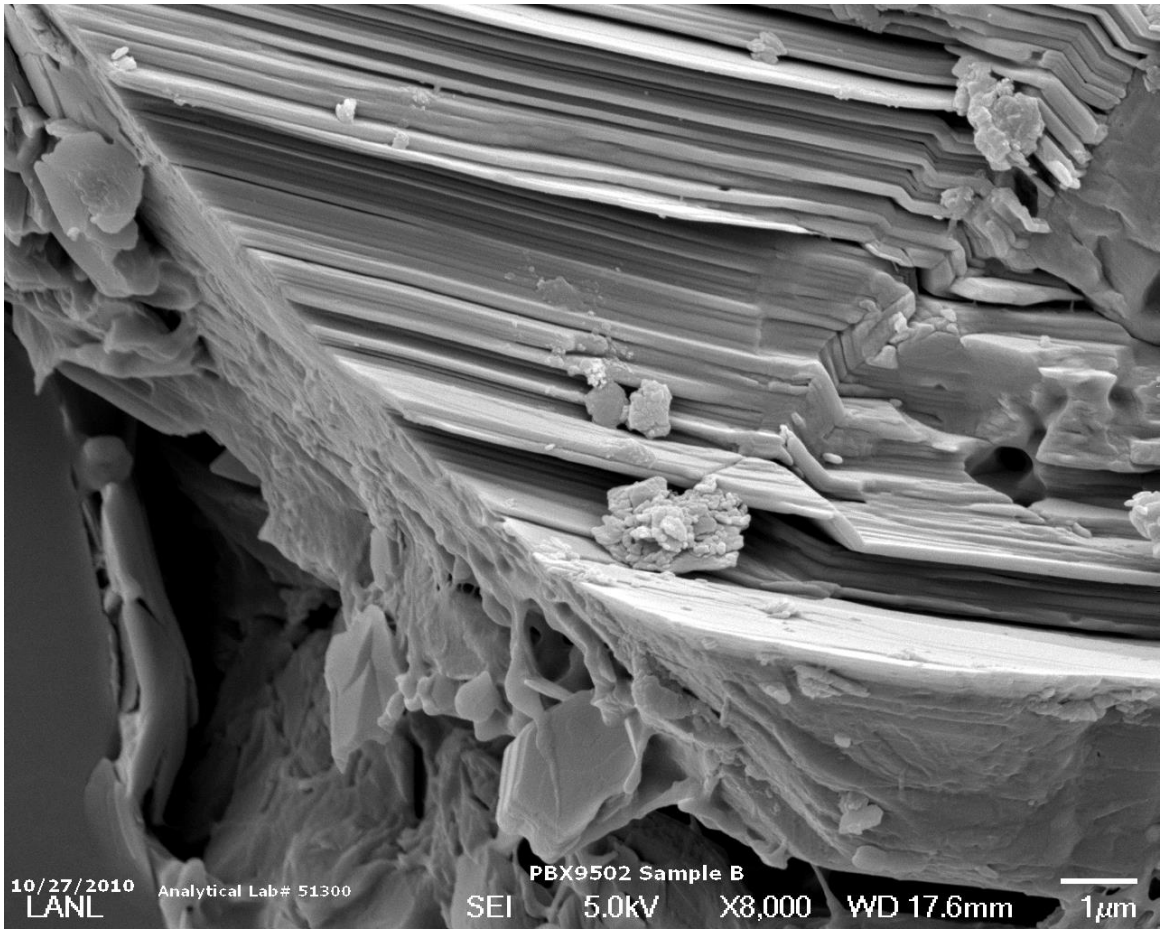

Figure 1. Scanning Electron Micrograph of the fracture surface of a pressed PBX 9502 part.

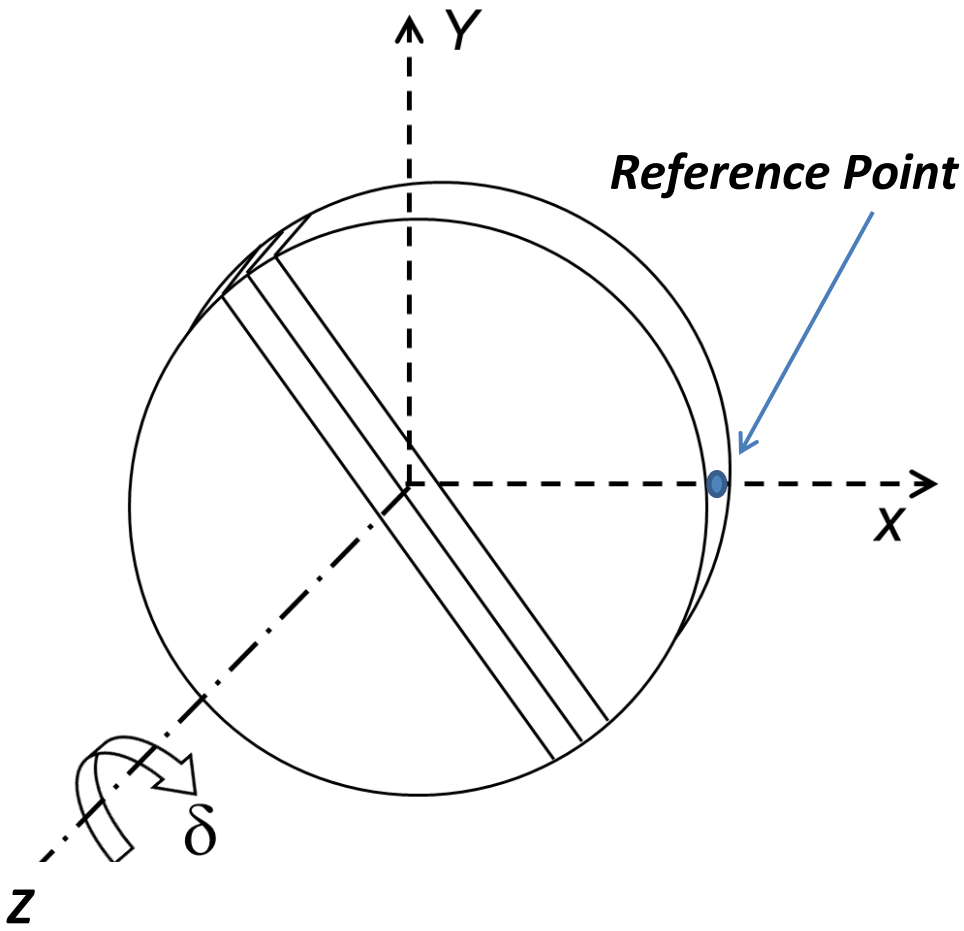

Figure 2. Schematic of the coordinate system attached to the specimen.

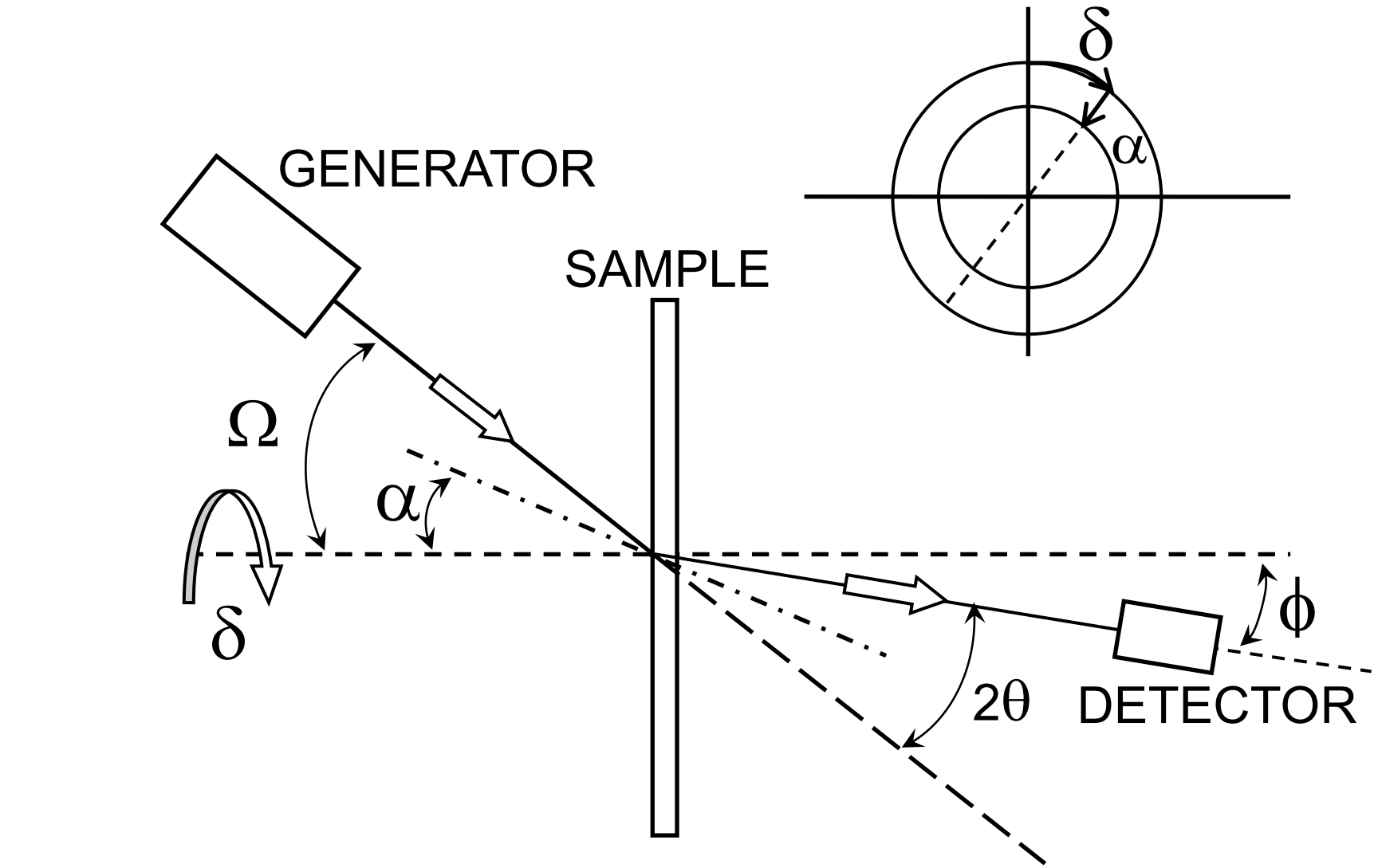

Fig. 3. Schematic describing the collection of texture data via the transmission method of Decker, Asp, and Harker (1948)

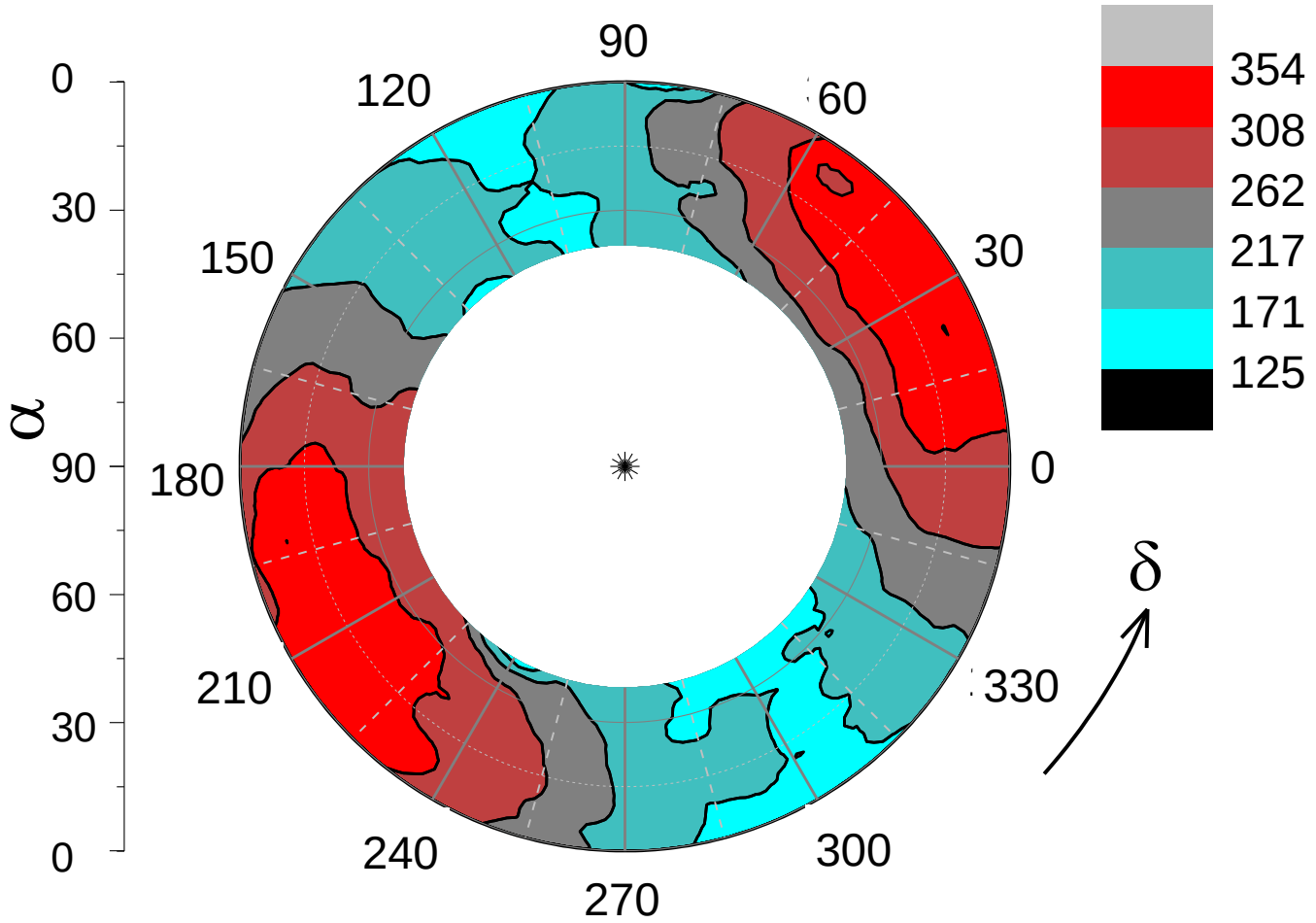

Figure 4. (002) Pole Figure for the PBX 9502 disc specimen.

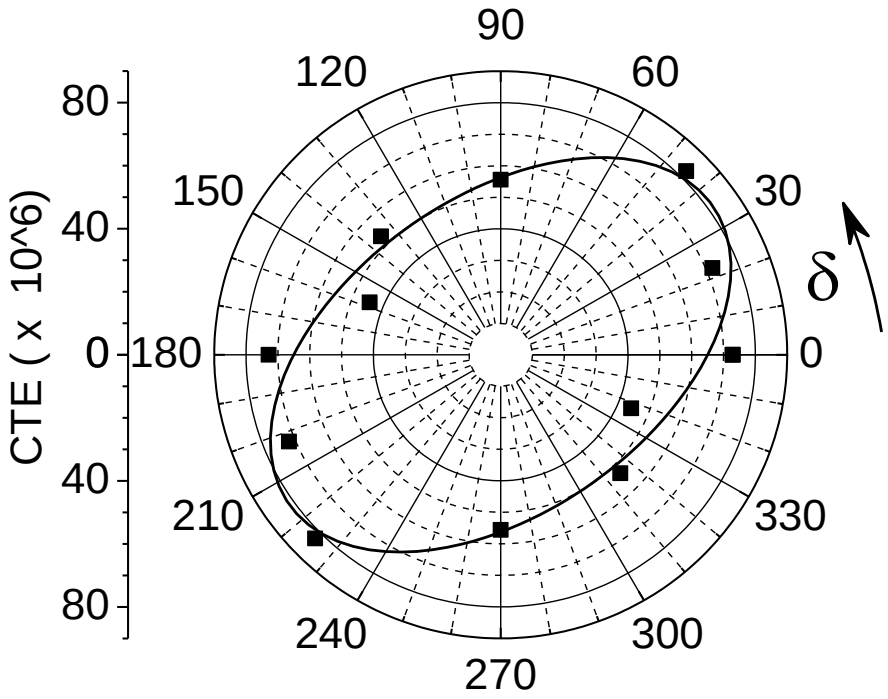

Figure 5. CTE measured across the diameter of the PBX 9502 disk. The angle δ gives the orientation of the diameter, as defined in Fig. 2.

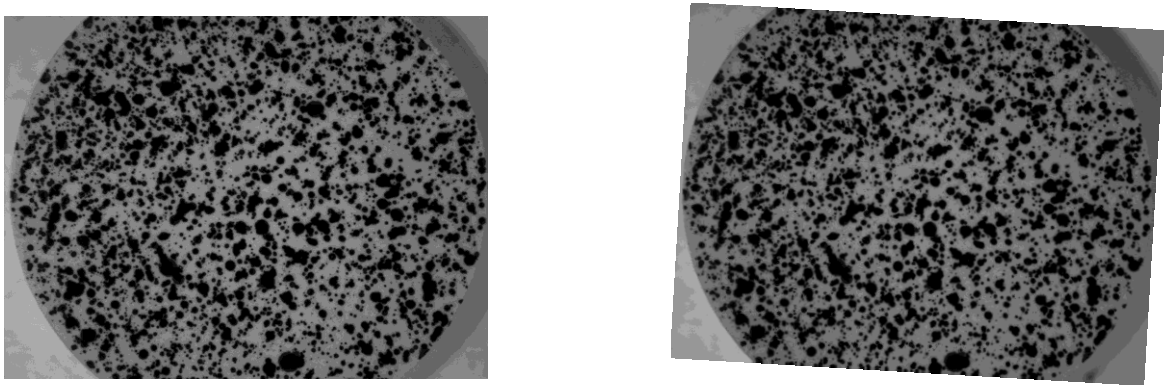

Figure 6. Speckle images of the testing disk: (a) Before ratchet growth and (b) after ratchet growth.

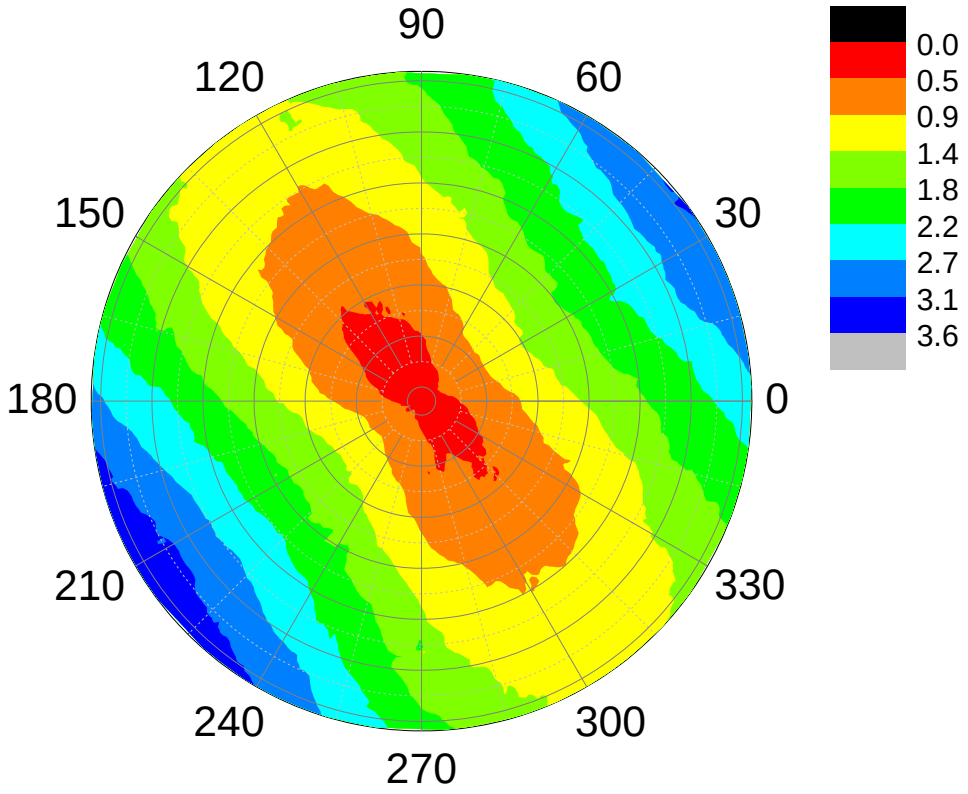

Figure 7. Radial displacement, u_r, on the surface of the PBX 9502 disk. The color-coded scale is in pixel units (1 pixel = 8 μm).

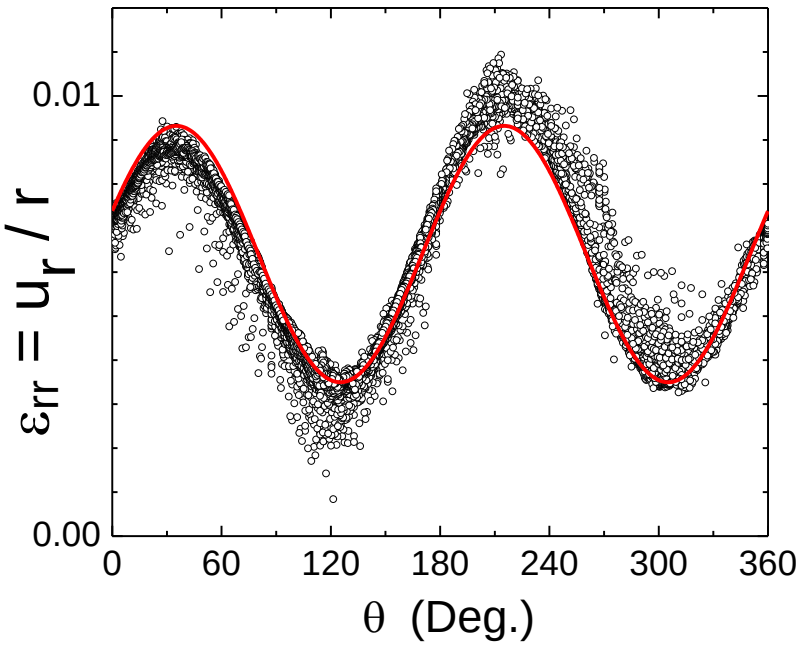

Figure 8. Ratio u_r/r for all points on the disk surface, as a function of the angle θ.

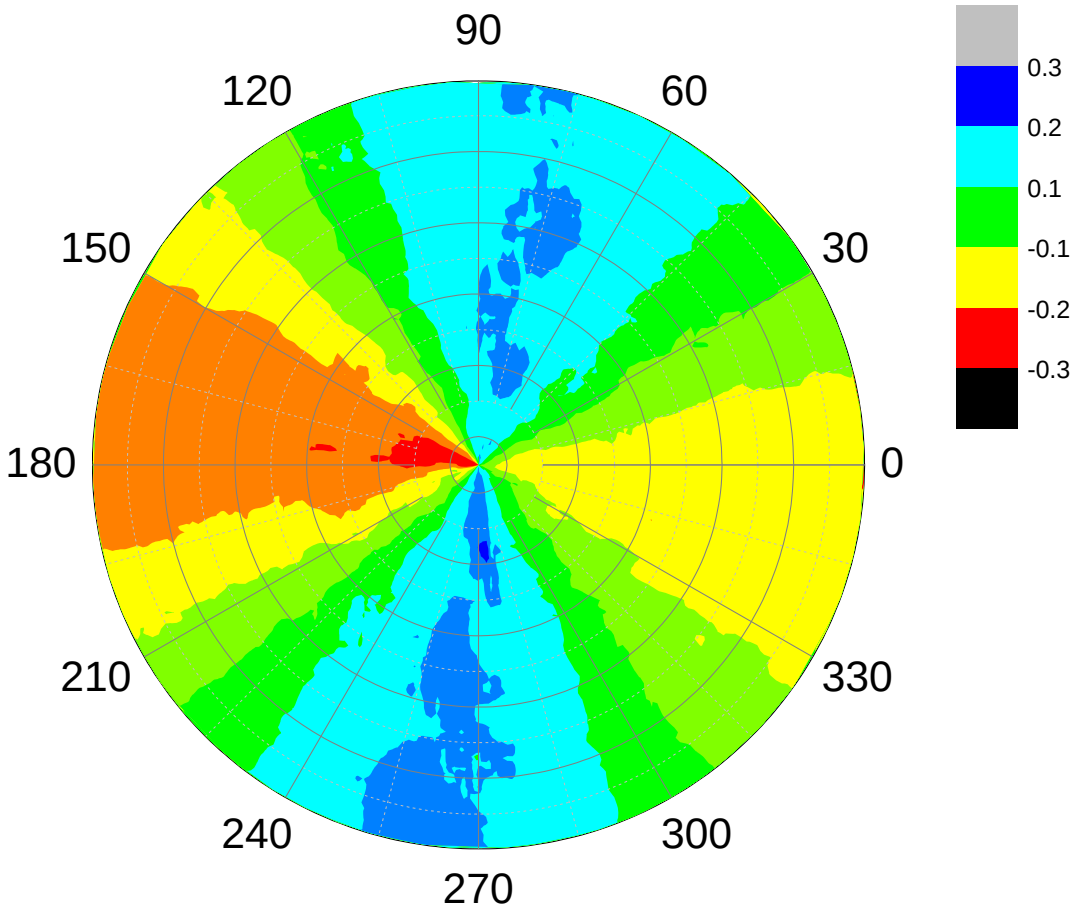

Figure 9. Angular displacement, $\Delta\theta$, on the surface of the PBX 9502 disk. The color-coded scale is in degree.

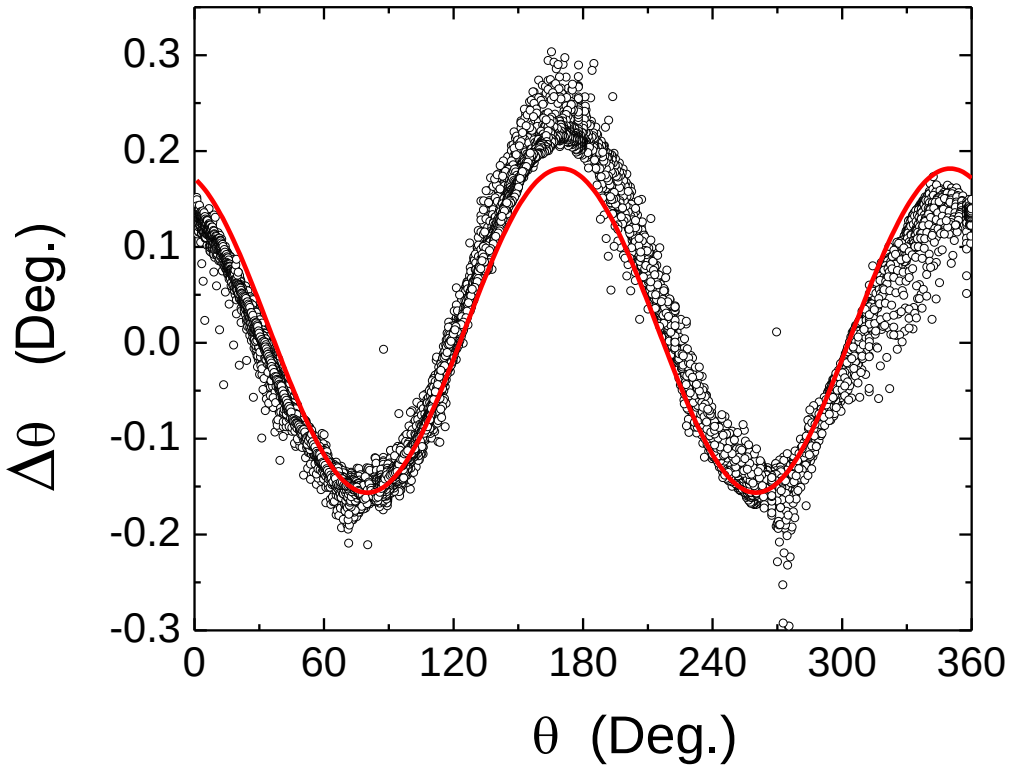

Figure10. Angular displacement, $\Delta\theta$, for all points on the disk surface, as a function of the angle θ.

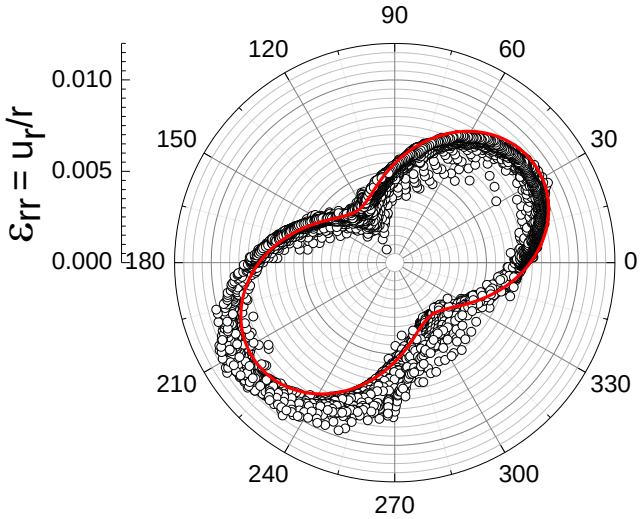

Figure 11. Polar plot of the radial component of ratchet growth strain, $\varepsilon_{rr} = u_r/r$, on the surface of the disk of PBX 9502.

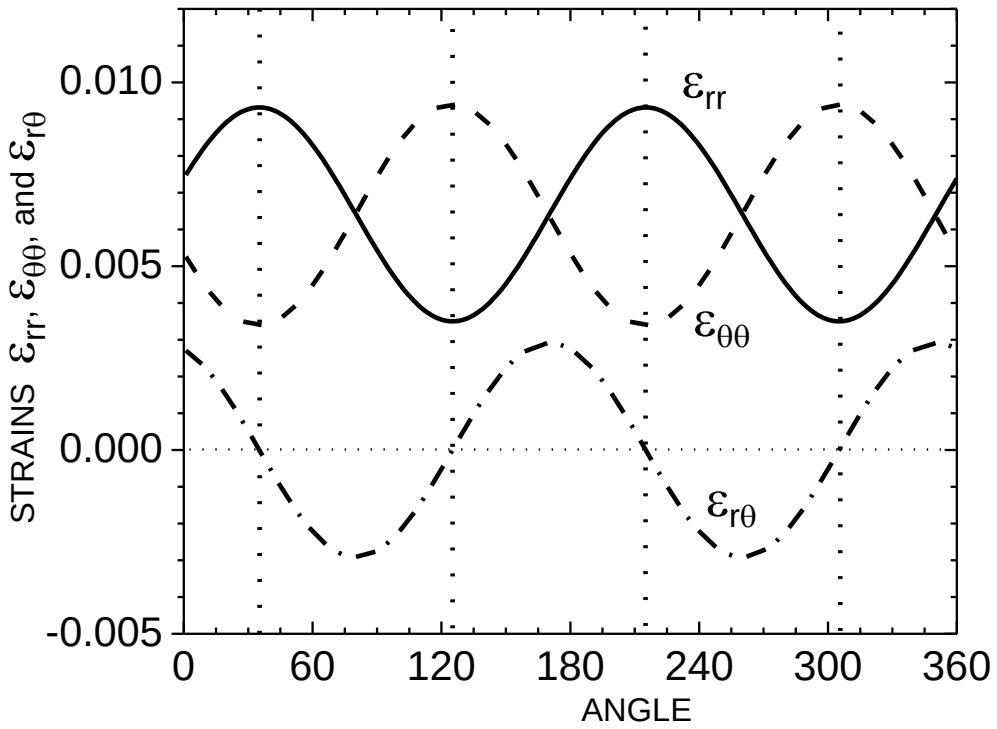

Figure 12. Strain components ε_{rr}, $\varepsilon_{\theta\theta}$, and $\varepsilon_{r\theta}$ caused by ratchet growth in the disk-shaped PBX 9502 disk.

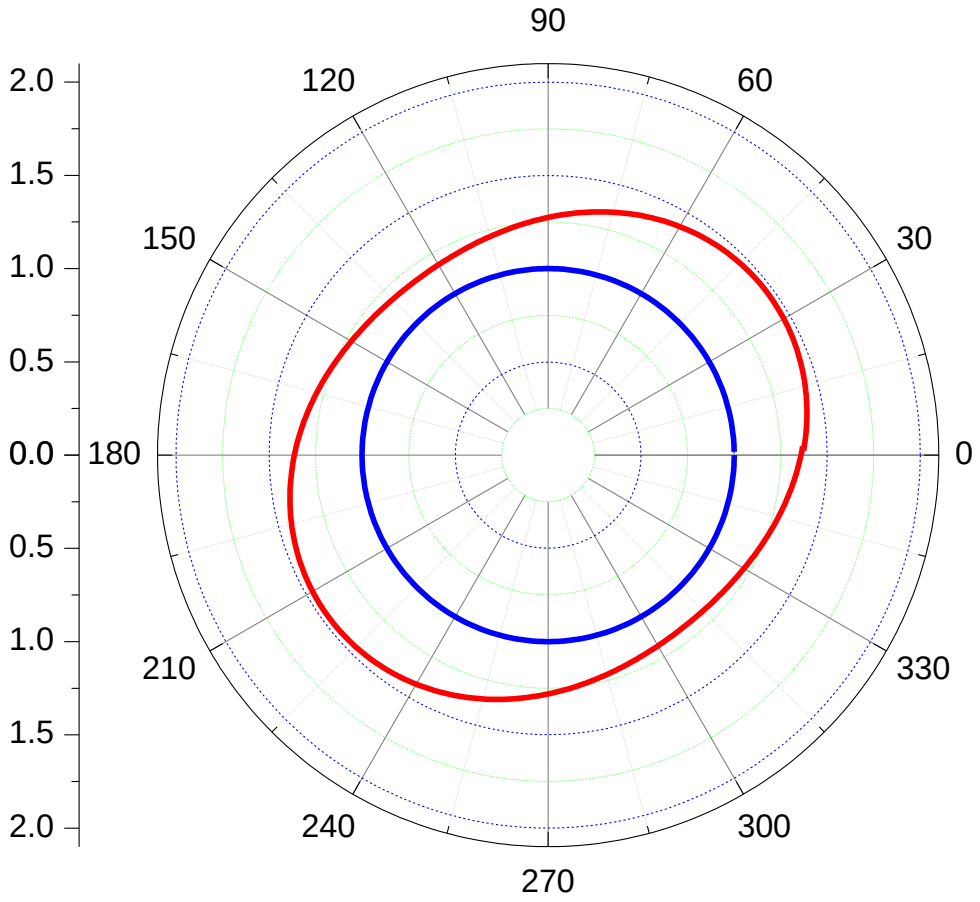

Figure 13. Deformation of the PBX 9502 disk. Blue: shape before ratchet growth. Red: shape after ratchet growth. To better illustrate the effect, the radial strain component, ε_{rr}, has been amplified by a factor of 50.

ε_o	ε_1	θ_r	Δ_o	Δ_1	θ_θ
		Deg.	Deg.	Deg.	Deg.
0.0064	0.0029	70.3	–0.01272	–0.1685	70.0

Table 1. Numerical values for the parameters in the fitted equations.